

Extrinsic Calibration of Multiple Inertial Sensors from Arbitrary Trajectories

Jongwon Lee¹, David Hanley², and Timothy Bretl¹

Abstract—We present a method of extrinsic calibration for a system of multiple inertial measurement units (IMUs) that estimates the relative pose of each IMU on a rigid body using only measurements from the IMUs themselves, without the need to prescribe the trajectory. Our method is based on solving a nonlinear least-squares problem that penalizes inconsistency between measurements from pairs of IMUs. We validate our method with experiments both in simulation and in hardware. In particular, we show that it meets or exceeds the performance—in terms of error, success rate, and computation time—of an existing, state-of-the-art method that does not rely only on IMU measurements and instead requires the use of a camera and a fiducial marker. We also show that the performance of our method is largely insensitive to the choice of trajectory along which IMU measurements are collected.

I. INTRODUCTION

Inertial sensors are widely used in mobile robot navigation systems. These sensors are typically packaged in an inertial measurement unit (IMU), which consists of a triaxial accelerometer to measure specific force along orthogonal axes and of three gyroscopes to measure angular rates about these same axes. While it is still common to use only a single IMU as the basis for a navigation system, it has been recognized that the simultaneous use of multiple IMUs on the same robot may result in higher measurement accuracy, increased bandwidth, and better fault tolerance than could have been achieved with a single IMU of the same total size, weight, power, and cost [1]–[7]. In order to realize these benefits, however, it is necessary to perform *extrinsic calibration*—that is, to estimate the relative position and orientation (i.e., the relative *pose*) of each IMU with respect to the robot on which they are all mounted.

Existing methods of extrinsic calibration for multi-IMU systems fall into three categories. First, there are methods that rely on the use of instruments (e.g., rate tables) to precisely control the trajectory of the robot on which the IMUs are mounted [8]–[11]. Calibration is then a matter of choosing the relative pose of each IMU that minimizes the difference between expected and actual measurements. We largely ignore methods in this first category, since our goal in this paper is to perform extrinsic calibration from data collected in flight along arbitrary trajectories. Second, there are methods that rely on the use of aiding sensors, for example a camera. “Kalibr” is one such method—it

TABLE I: COMPARING DIFFERENT METHODS OF EXTRINSIC CALIBRATION FOR MULTIPLE IMUS

method	characteristics			estimated quantities		
	free from camera?	arbitrary trajectory?	code available?	p	q	$\frac{g}{I}q$
Qui <i>et al.</i> [14]	•	•	-	-	•	-
Kim <i>et al.</i> [15]	•	•	-	•	•	-
Schopp <i>et al.</i> [16]	•	•	-	•	•	-
Rehder <i>et al.</i> [13]	-	-	•	•	•	•
Kortier [17]	•	-	-	•	•	•
Our Method	•	•	•	•	•	•

p: IMU position, q: IMU orientation, $\frac{g}{I}q$: gyroscope misalignment,
•: applicable, -: not applicable

assumes the navigation system consists of a single camera and of multiple IMUs, and applies well-known algorithms to estimate the pose of each IMU (one-by-one) with respect to the camera, given images of fiducial markers [12], [13]. Again, we largely ignore methods in this second category, since our goal in this paper is to perform extrinsic calibration without the use of aiding sensors. However, we do use Kalibr as a benchmark in our hardware experiments (Section IV), since it is available as open-source and provides excellent performance. Third, there are methods that—like ours—require neither instruments nor aiding sensors [14]–[17]. Instead, these methods require only measurements from the IMUs themselves. We were particularly inspired by the method of Schopp *et al.* [16], which—like ours—is based on solving a nonlinear least-squares problem that penalizes inconsistency between expected and actual measurements. Indeed, one way to think about what we are trying to do in this paper is to extend methods in this third category to eliminate certain limitations (e.g., applying only to arrays of accelerometers and not gyroscopes) and to relax certain assumptions (e.g., that accelerometer and gyroscope axes are perfectly aligned in each IMU).

Section II presents our method of extrinsic calibration. Section III validates our method with experimental results in simulation using OpenVINS [18]. Section IV validates our method with experimental results in hardware, using Kalibr as a benchmark. Section V discusses a number of directions for future work.

Both the code and dataset used in this paper are available online.¹

¹Jongwon Lee and Timothy Bretl are with the Department of Aerospace Engineering, University of Illinois at Urbana-Champaign, Urbana, IL 61801, USA (Email: {jongwon5, tbretl}@illinois.edu).

²David Hanley is with the Department of Electrical and Computer Engineering, University of Illinois at Urbana-Champaign, Urbana, IL 61801, USA (Email: hanley6@illinois.edu).

¹<https://github.com/jongwonlee/mix-cal>

II. METHODOLOGY

A. Notation

We use ${}^B_A\mathbf{R} \in SO(3)$ to denote the rotation matrix that describes the orientation of frame \mathcal{F}_A in the coordinates of frame \mathcal{F}_B . We use $\mathbf{C}(\cdot)$ to denote the operator that converts a unit quaternion ${}^B_A\mathbf{q}$ to the corresponding rotation matrix ${}^B_A\mathbf{R}$. Coordinate transformations are expressed as follows:

$${}^B\mathbf{p} = {}^B_A\mathbf{R} {}^A\mathbf{p} = \mathbf{C}({}^B_A\mathbf{q}) {}^A\mathbf{p}.$$

We will use the following symbols to distinguish between different types of quantities:

- a tilde $\widetilde{(\cdot)}$ means a sensor measurement,
- a hat $\widehat{(\cdot)}$ means an estimate,
- a zero superscript $(\cdot)^0$ means an initial guess (before optimization),
- and an asterisk superscript $(\cdot)^*$ means a final value (after optimization).

B. Inertial sensor model

We model the accelerometer measurements from each IMU as

$${}^I\tilde{\mathbf{a}} = {}^I\mathbf{a}_{WI} - {}^I\mathbf{g} + \mathbf{b}_a + \mathbf{n}_a \quad (1)$$

where

- ${}^I\mathbf{a}_{WI}$ is the linear acceleration of the IMU frame with respect to the world frame, expressed in the IMU frame,
- ${}^I\mathbf{g}$ is the acceleration of gravity expressed in the IMU frame,
- \mathbf{b}_a is a time-varying bias that is described by a random walk

$$\mathbf{b}_{a,k+1} - \mathbf{b}_{a,k} \sim \sigma_{\mathbf{b}_a} \sqrt{\Delta t} \cdot \mathcal{N}(\mathbf{0}, \mathbf{1}),$$

- and \mathbf{n}_a is stochastic noise

$$\mathbf{n}_a \sim \sigma_a / \sqrt{\Delta t} \cdot \mathcal{N}(\mathbf{0}, \mathbf{1})$$

where Δt is the sampling interval of the IMU. We model the gyroscope measurements from each IMU as

$${}^g\tilde{\omega} = \mathbf{C}({}^g_I\mathbf{q}) {}^I\omega_{WI} + \mathbf{b}_g + \mathbf{n}_g \quad (2)$$

where

- $\mathbf{C}({}^g_I\mathbf{q})$ is the rotation matrix (written in terms of the corresponding quaternion) that describes the orientation of the IMU frame with respect to the gyroscope frame and that allows us to model gyroscope misalignment,
- ${}^I\omega_{WI}$ is the angular velocity of the IMU frame with respect to the world frame, expressed in the IMU frame,
- \mathbf{b}_g is a time-varying bias that is described by a random walk

$$\mathbf{b}_{g,k+1} - \mathbf{b}_{g,k} \sim \sigma_{\mathbf{b}_g} \sqrt{\Delta t} \cdot \mathcal{N}(\mathbf{0}, \mathbf{1}),$$

- and \mathbf{n}_g is stochastic noise

$$\mathbf{n}_g \sim \sigma_g / \sqrt{\Delta t} \cdot \mathcal{N}(\mathbf{0}, \mathbf{1}).$$

In what follows, we assume the square roots of noise density σ_a , σ_g and bias instability $\sigma_{\mathbf{b}_a}$, $\sigma_{\mathbf{b}_g}$ in continuous-time have been identified for all sensors prior to extrinsic calibration.

We choose not to include the non-orthogonality and scale factors of both the accelerometers and gyroscopes in our calibration process. These parameters can be calibrated in advance using one of several existing approaches [19]–[22]. We do, on the other hand, model gyroscope misalignment which is frequently ignored in existing calibration processes [21], [22]. We show in Section III that including these parameters in our calibration process can reduce the RMSE of the remaining calibration parameters. In addition, we choose not to include time offset parameters or asynchronous measurements in our calibration process. There exist several approaches to estimate these parameters separately in software or to correct these issues in hardware [23]–[25].

C. Problem statement (multi-IMU extrinsic calibration)

Suppose there are $N + 1$ IMUs and that we index the frames attached to each of these IMUs as

$$I_0, \dots, I_N.$$

We use ${}^{I_0}\mathbf{p}_{I_0 I_n} := \mathbf{p}_{I_n}$ to denote the relative position of frame I_n with respect to frame I_0 , written in the coordinates of frame I_0 . We use ${}^{I_0}_{I_n}\mathbf{q} := \mathbf{q}_{I_n}$ to denote the quaternion describing the relative orientation of frame I_n with respect to frame I_0 . Note that these IMU frames I_0, \dots, I_N are assumed to be aligned with the accelerometers. Gyroscopes measurements are taken in frames g_0, \dots, g_N , where a given frame g_n is misaligned from the IMU frame I_n by quaternion ${}^{g_n}_{I_n}\mathbf{q}$. Given a sequence of measurements

$${}^{I_n}\tilde{\mathbf{a}}_k, {}^{g_n}\tilde{\omega}_k$$

at each time $k \in \{1, \dots, K\}$ for each IMU $n \in \{0, \dots, N\}$, the goal of extrinsic calibration is to estimate the parameters

$$\begin{aligned} & \mathbf{p}_{I_1}, \dots, \mathbf{p}_{I_N} \\ & \mathbf{q}_{I_1}, \dots, \mathbf{q}_{I_N} \\ & {}^{g_0}_{I_0}\mathbf{q}, {}^{g_1}_{I_1}\mathbf{q}, \dots, {}^{g_N}_{I_N}\mathbf{q}. \end{aligned}$$

To facilitate the estimation of these extrinsic parameters, we have found that it is helpful to simultaneously estimate the time-varying accelerometer and gyroscope biases

$$\mathbf{b}_{a_n, k}, \mathbf{b}_{g_n, k}$$

at each time $k \in \{1, \dots, K\}$ for each IMU $n \in \{0, \dots, N\}$, as well as the angular acceleration of the base IMU

$${}^{I_0}\boldsymbol{\alpha}_{WI_0, k} := {}^{I_0} \boldsymbol{\alpha}_k$$

at each time $k \in \{1, \dots, K\}$. These extra parameters can be thought of as auxiliary or slack variables. Note that we do not attempt to estimate the full trajectory of the rigid body to which the IMUs are mounted.

D. Solution approach (maximum-likelihood estimation)

Defining $\mathcal{X}_{0,k} = \{{}^{g_0}_{I_0}\mathbf{q}, \mathbf{b}_{a_0, k}, \mathbf{b}_{g_0, k}, {}^{I_0}\boldsymbol{\alpha}_k\}$ and $\mathcal{X}_{n,k} = \{\mathbf{p}_{I_n}, \mathbf{q}_{I_n}, {}^{g_n}_{I_n}\mathbf{q}, \mathbf{b}_{a_n, k}, \mathbf{b}_{g_n, k}\}$, the overall parameters $\mathcal{X} =$

$\{\mathcal{X}_{n,k} \mid n \in \{0, \dots, N\}, k \in \{1, \dots, K\}\}$ can be estimated by solving a non-linear least-square problem

$$\begin{aligned} \min_{\mathcal{X}} & \left\{ \sum_{\substack{n \in \{1, \dots, N\} \\ k \in \{1, \dots, K\}}} \left(\|\mathbf{r}_a(\mathcal{X}_{n,k}, \mathcal{X}_{0,k}; {}^{I_n}\tilde{\mathbf{a}}_k, {}^{I_0}\tilde{\mathbf{a}}_k, {}^{g_0}\tilde{\boldsymbol{\omega}}_k)\|_{\Sigma_a}^2 \right. \right. \\ & + \|\mathbf{r}_g(\mathcal{X}_{n,k}, \mathcal{X}_{0,k}; {}^{g_n}\tilde{\boldsymbol{\omega}}_k, {}^{g_0}\tilde{\boldsymbol{\omega}}_k)\|_{\Sigma_g}^2 \left. \left. \right) \right. \\ & + \sum_{\substack{n \in \{0, \dots, N\} \\ k \in \{1, \dots, K-1\}}} \left(\|\mathbf{r}_{\mathbf{b}_a}(\mathcal{X}_{n,k})\|_{\Sigma_{\mathbf{b}_a}}^2 \right. \\ & \left. \left. + \|\mathbf{r}_{\mathbf{b}_g}(\mathcal{X}_{n,k})\|_{\Sigma_{\mathbf{b}_g}}^2 \right) \right) \end{aligned} \quad (3)$$

where $\|\cdot\|_{\Sigma}^2$ denotes Mahalanobis distance with a covariance matrix Σ .

The residual \mathbf{r}_a relates the n th accelerometer's measurement (${}^{I_n}\tilde{\mathbf{a}}_k$) compensated by its bias ($\mathbf{b}_{a,n,k}$) to the specific force reconstructed by the base IMU measurement (${}^{I_n}\hat{\mathbf{a}}_k$)

$$\mathbf{r}_a = ({}^{I_n}\tilde{\mathbf{a}}_k - \mathbf{b}_{a,n,k}) - {}^{I_n}\hat{\mathbf{a}}_k.$$

${}^{I_n}\hat{\mathbf{a}}_k$ is formulated by mapping the specific force at base IMU into the n th IMU, parametrized by their geometric relationship and rotational motion

$$\begin{aligned} {}^{I_n}\hat{\mathbf{a}}_k &= {}^{I_0}\mathbf{R}^{-1} \left\{ {}^{I_0}\hat{\mathbf{a}}_k + [{}^{I_0}\tilde{\boldsymbol{\omega}}_k]_{\times} \mathbf{p}_{I_n} + [{}^{I_0}\boldsymbol{\alpha}_k]_{\times} \mathbf{p}_{I_n} \right\}, \\ {}^{I_0}\hat{\mathbf{a}}_k &= {}^{I_0}\tilde{\mathbf{a}}_k - \mathbf{b}_{a_0,k}, \quad {}^{I_0}\tilde{\boldsymbol{\omega}}_k = {}^{g_0}\mathbf{R}^{-1}({}^{g_0}\tilde{\boldsymbol{\omega}}_k - \mathbf{b}_{g_0,k}) \end{aligned}$$

where ${}^{I_n}\mathbf{R} = \mathbf{C}(\mathbf{q}_{I_n})$, ${}^{g_0}\mathbf{R} = \mathbf{C}({}^{g_0}\mathbf{q})$. Note that $[\cdot]_{\times}$ is an operator converting a cross product into a skew-symmetric matrix form. As the sensor measurement subtracted by their own bias has an uncertainty due to zero-mean gaussian white noise—i.e. $\tilde{\mathbf{a}} - \mathbf{b}_a = \mathbf{n}_a$ from Eq. (1) and $\tilde{\boldsymbol{\omega}} - \mathbf{b}_g = \mathbf{n}_g$ from Eq. (2), the corresponding covariance matrix for \mathbf{r}_a is $\Sigma_a = \{2 \cdot \sigma_a^2 / \Delta t + (\sigma_g^2 / \Delta t)^2\} \cdot \mathbf{I}_{3 \times 3}$.

\mathbf{r}_g is a residual relating the n th gyroscope's measurement (${}^{g_n}\tilde{\boldsymbol{\omega}}_k$) to that of base gyroscope's (${}^{g_0}\tilde{\boldsymbol{\omega}}_k$), both of which are compensated by their own biases ($\mathbf{b}_{g_n,k}$, $\mathbf{b}_{g_0,k}$)

$$\begin{aligned} \mathbf{r}_g &= {}^{I_0}\tilde{\boldsymbol{\omega}}_{WI_n} - {}^{I_0}\hat{\boldsymbol{\omega}}_{WI_n} \\ &= {}^{I_n}\mathbf{R} {}^{I_n}\mathbf{R}^{-1}({}^{g_n}\tilde{\boldsymbol{\omega}}_k - \mathbf{b}_{g_n,k}) - {}^{g_0}\mathbf{R}^{-1}({}^{g_0}\tilde{\boldsymbol{\omega}}_k - \mathbf{b}_{g_0,k}) \end{aligned}$$

where ${}^{I_n}\mathbf{R} = \mathbf{C}(\mathbf{q}_{I_n})$, ${}^{g_n}\mathbf{R} = \mathbf{C}({}^{g_n}\mathbf{q})$, and ${}^{g_0}\mathbf{R} = \mathbf{C}({}^{g_0}\mathbf{q})$. This relation holds as the same rotational motion is experienced at any locations on the same rigid body. Similar to the covariance matrix for \mathbf{r}_a , the covariance matrix for \mathbf{r}_g is $\Sigma_g = 2\sigma_g^2 / \Delta t \cdot \mathbf{I}_{3 \times 3}$. Note that \mathbf{r}_a and \mathbf{r}_g both take ${}^{g_0}\tilde{\boldsymbol{\omega}}_k$ as input and therefore are correlated.

$\mathbf{r}_{\mathbf{b}_a}$ and $\mathbf{r}_{\mathbf{b}_g}$ accounts for bias evolution along time

$$\begin{aligned} \mathbf{r}_{\mathbf{b}_a} &= \mathbf{b}_{a_n,k+1} - \mathbf{b}_{a_n,k} \\ \mathbf{r}_{\mathbf{b}_g} &= \mathbf{b}_{g_n,k+1} - \mathbf{b}_{g_n,k}. \end{aligned}$$

These residuals' covariance matrices $\Sigma_{\mathbf{b}_a}$, $\Sigma_{\mathbf{b}_g}$ comes from the bias evolution in discretized time domain; hence, $\Sigma_{\mathbf{b}_a} = \sigma_{\mathbf{b}_a}^2 \Delta t \cdot \mathbf{I}_{3 \times 3}$, $\Sigma_{\mathbf{b}_g} = \sigma_{\mathbf{b}_g}^2 \Delta t \cdot \mathbf{I}_{3 \times 3}$.

E. Degenerate cases

The solution to Eq. (3) can be found when the Fisher information matrix (FIM) is invertible [26]. This is identical to the condition when the Jacobian of Eq. (3),

$$\mathbf{J} = \begin{bmatrix} \mathbf{J}_{1,0} & \mathbf{J}_{1,1} & \cdots & \mathbf{J}_{1,N} \\ \mathbf{J}_{2,0} & \mathbf{J}_{2,1} & \cdots & \mathbf{J}_{2,N} \\ \vdots & \vdots & \ddots & \vdots \\ \mathbf{J}_{K,0} & \mathbf{J}_{K,1} & \cdots & \mathbf{J}_{K,N} \end{bmatrix}$$

composed of submatrices at each time $k \in \{1, \dots, K\}$ for each IMU $n \in \{0, \dots, N\}$

$$\mathbf{J}_{k,n} = \begin{cases} \begin{bmatrix} \frac{\partial \mathbf{r}_a}{\partial \mathbf{x}_0} & \frac{\partial \mathbf{r}_g}{\partial \mathbf{x}_0} & \frac{\partial \mathbf{r}_{b_a}}{\partial \mathbf{x}_0} & \frac{\partial \mathbf{r}_{b_g}}{\partial \mathbf{x}_0} \end{bmatrix}^T \in \mathbb{R}^{12 \times 12} & \text{if } k \neq K, n = 0 \\ \begin{bmatrix} \frac{\partial \mathbf{r}_a}{\partial \mathbf{x}_n} & \frac{\partial \mathbf{r}_g}{\partial \mathbf{x}_n} & \frac{\partial \mathbf{r}_{b_a}}{\partial \mathbf{x}_n} & \frac{\partial \mathbf{r}_{b_g}}{\partial \mathbf{x}_n} \end{bmatrix}^T \in \mathbb{R}^{12 \times 15} & \text{if } k \neq K, n \neq 0 \\ \begin{bmatrix} \frac{\partial \mathbf{r}_a}{\partial \mathbf{x}_0} & \frac{\partial \mathbf{r}_g}{\partial \mathbf{x}_0} \end{bmatrix}^T \in \mathbb{R}^{6 \times 12} & \text{if } k = K, n = 0 \\ \begin{bmatrix} \frac{\partial \mathbf{r}_a}{\partial \mathbf{x}_n} & \frac{\partial \mathbf{r}_g}{\partial \mathbf{x}_n} \end{bmatrix}^T \in \mathbb{R}^{6 \times 15} & \text{if } k = K, n \neq 0 \end{cases}$$

is full rank. In this paper, we do not derive all cases where this condition breaks, which we call degenerate cases. However, degenerate cases do exist. The exact set of degenerate cases will vary with respect to the number of IMUs, their geometric arrangement, the number of timesteps, the distribution of measurement, and more.

Previous work on the self-calibration for camera-IMU systems [27], [28] find that motions such as constant acceleration or rotation along a single axis at a constant rate result in a failure mode. In line with this, we run our experiments (wherein we compare our IMU extrinsic calibration techniques to a camera-IMU system) on trajectories where such motions are avoided.

III. SIMULATION EXPERIMENTS

To verify the robustness of our multi-IMU extrinsic calibration along arbitrary trajectories as stated above, we performed several experiments using OpenVINS [18], an open-source visual-inertial simulator. It is commonly the case that engineering drawings dictate a reasonable initial guess for the (nominal) position and orientation of a set of sensors, but manufacturing tolerances place the sensors at different locations and orientations. Therefore, our robustness evaluation considers sensors placed at a nominal position with initial guesses for parameter estimates selected according to samples from a Gaussian distribution about these nominal positions and orientations. Then we consider the robustness of our solutions where the initial guess for extrinsic parameters may be well outside these tolerances. We show that, even outside typical manufacturing tolerances, our method is robust to different initial conditions.

A. Implementation details

We assumed that four IMUs were mounted to a rigid body. Table II shows the reference pose of each IMU. The accelerometers' noise and random walk characteristics were $\sigma_a = 2 \times 10^{-3} \text{ m/s}^2 / \sqrt{\text{Hz}}$ and $\sigma_{\mathbf{b}_a} = 3 \times 10^{-3} \text{ m/s}^2 \cdot \sqrt{\text{Hz}}$, while those of gyroscopes were $\sigma_g = 1.6968 \times 10^{-4} \text{ rad/s} / \sqrt{\text{Hz}}$ and $\sigma_{\mathbf{b}_g} = 1.9393 \times 10^{-5} \text{ rad/s} \cdot \sqrt{\text{Hz}}$. The first values of simulated time-varying biases $\mathbf{b}_{a_n,1}$ and $\mathbf{b}_{g_n,1}$

TABLE II: REFERENCE IMU POSES IN SIMULATION

index	position [mm]	orientation [rad]*
IMU0	[0, 0, 0]	[0, 0, 0]
IMU1	[200, 0, 0]	[\pi, 0, 0]
IMU2	[0, 200, 0]	[0, \pi, 0]
IMU3	[0, 0, 200]	[0, 0, \pi]

* in this table, orientation is given as XYZ Euler angles

were sampled from a uniform distribution on the interval $[-0.05, 0.05]$. Gyroscope misalignment was generated by rotating the reference orientation of each IMU about an axis chosen uniformly at random by an angle sampled from a zero-mean normal distribution with standard deviation of 1° . IMU measurements were generated at 100 Hz and have synchronized time stamps while the rigid body was moved along six different trajectories from the TUM-VI Dataset [29]. Fig 1 shows one of these trajectories.

B. Results when initial guesses are within typical manufacturing tolerances

Table III shows the root mean square error (RMSE) of the estimated extrinsic parameters—the relative position \mathbf{p}_{I_n} and orientation \mathbf{q}_{I_n} of each IMU $n \in \{1, \dots, N\}$ with respect to the base IMU0—over twenty trials along each trajectory in the case when initial guesses were within typical manufacturing tolerances. The initial guess of each relative position was sampled from a normal distribution with mean equal to the reference position and with a standard deviation along each axis of 5 mm. The initial guess of each relative orientation was generated by rotating the reference orientation about an axis chosen uniformly at random by an angle sampled from a zero-mean normal distribution with a standard deviation of 5° . Our results show that, when we included gyroscope misalignment ${}^g_I \mathbf{q}$ in the set of parameters to be estimated (with an initial guess of zero misalignment), our proposed method achieved sub-millimeter and sub-degree error for all trajectories, which is comparable to other existing methods [15], [16]. Our results also show, in particular, that it is important to estimate gyroscope misalignment (something that not all methods listed in Table I do, for example Kim *et al.*[15])—without estimating misalignment, position and orientation errors were between one and two orders of magnitude higher.

Table IV shows the RMSE of the estimated angular accelerations ${}^{I_0} \alpha_k^*$ and time-varying biases $\mathbf{b}_{a_{n,k}}^*$, $\mathbf{b}_{g_{n,k}}^*$ for each time $k \in \{1, \dots, K\}$ and each IMU $n \in \{0, \dots, N\}$ over the same twenty trials along each trajectory. The initial guess of each angular acceleration ${}^{I_0} \alpha_k^0$ was found by numerical differentiation of gyroscope measurements ${}^{g_0} \tilde{\omega}_k$ from the base IMU. The initial guess of each time-varying bias $\mathbf{b}_{a_{n,k}}^0$ and $\mathbf{b}_{g_{n,k}}^0$ was zero. Recall that angular accelerations and time-varying biases are extra parameters that we think of as auxiliary or slack variables and that their estimation is not our main focus. Nonetheless, results show that our proposed method reduces RMSE in estimates of all extra parameters

when compared to initial guesses. To help visualize these results, Fig. 2 shows the error of each estimated angular acceleration ${}^{I_0} \alpha_k^*$ and of each time-varying bias $\mathbf{b}_{a_{0,k}}^*$, $\mathbf{b}_{g_{0,k}}^*$ for the base IMU as functions of time over a single trial along each trajectory.

C. Results when initial guesses are outside typical manufacturing tolerances

Next, we study the extent to which the proposed method can reliably estimate extrinsic parameters when initial guesses are outside typical manufacturing tolerances.

Table V shows the RMSE of the estimated position between each IMU $n \in \{1, \dots, N\}$ with respect to IMU0 over the same twenty trajectories. Results are reported where the initial guesses for the relative position have between 0 and 30 mm error and initial guesses for relative orientation have between 0 and 90 degrees error. Our results show that—up to 60 degrees of error in the initial orientation and 30 mm of error in the initial relative position—relative position is estimated to within 0.2 millimeters.

Table VI shows the RMSE of the estimated orientation between each IMU $n \in \{1, \dots, N\}$ with respect to IMU0 over the same twenty trajectories. Again, results are reported where the initial guesses for the relative position have between 0 and 30 mm error and initial guesses for relative orientation have between 0 and 90 degrees error. Our results show that—up to 60 degrees of error in the initial orientation and 30 mm of error in the initial relative position—orientation is estimated to within 0.03 degrees.

Again, these initial errors are outside manufacturing tolerances considering the simulated platform’s scale as stated in Table II. Therefore, we conclude that our proposed method is robust to a poor initial guess of extrinsic parameters.

IV. HARDWARE EXPERIMENTS

In this section, we show that the proposed multi-IMU method can estimate extrinsic calibration parameters on par or better than Kalibr, a state-of-the-art and open-source calibration method [13]. In particular, because Kalibr relies upon camera images, it can perform poorly in ill-lit conditions or on trajectories that result in blurry images. The proposed method, because it does not use a camera, performs well despite these conditions. We demonstrate this point by comparing the performance of both methods for trajectories where the calibration image pattern—essential for using Kalibr—generally work well. Next we present calibration results for trajectories where blurry images and ill-lit conditions occur and may cause Kalibr to fail. All data and code are freely available online (see link in Section I).

A. Implementation details

Figure 3 shows the sensor rig that we used to collect a dataset with which to evaluate the performance of our method and of Kalibr. We placed two IMUs (labeled IMU0 and IMU1) and a camera (labeled CAM) on an optical breadboard. Each IMU consisted of one triaxial accelerometer (ST IIS3DWB) and three single-axis gyroscopes (Silicon Sensing

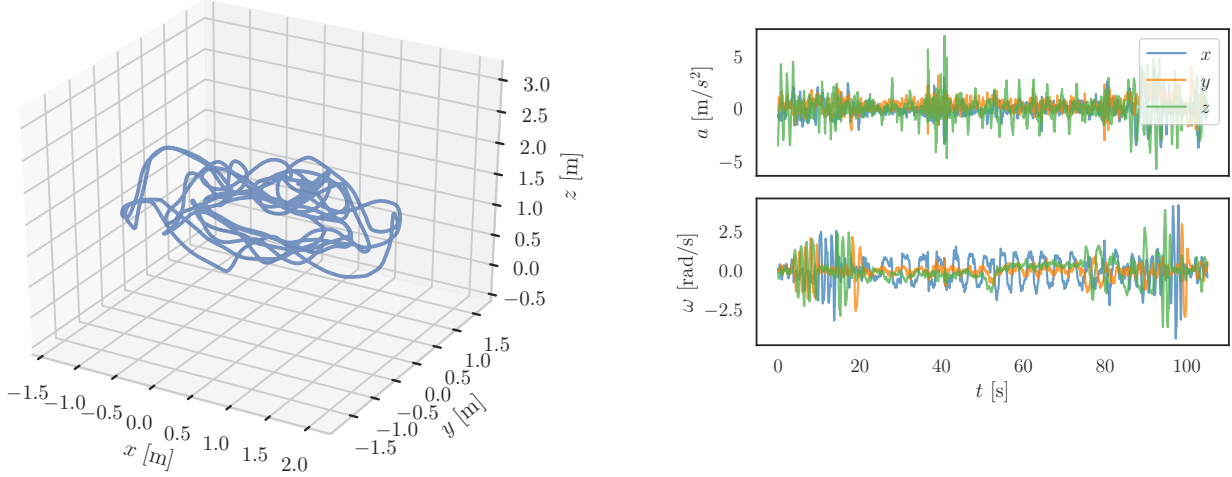


Fig. 1: An example trajectory for experiments in simulation (room4 in TUM-VI Dataset [29]).

TABLE III: RMSE OF ESTIMATED EXTRINSIC PARAMETERS OVER 20 TRIALS

trajectory	length [m]	duration [s]	Without Estimation of Gyroscope Misalignment		With Estimation of Gyroscope Misalignment		
			\mathbf{p} [mm]	\mathbf{q} [deg]	\mathbf{p} [mm]	\mathbf{q} [deg]	$g_I \mathbf{q}$ [deg]
room1	146.79	141.03	3.8003	1.6397	0.1704	0.0191	0.0391
room2	141.60	144.07	4.3648	2.0671	0.2318	0.0284	0.0422
room3	135.52	141.02	3.9474	1.1735	0.1445	0.0167	0.0353
room4	68.70	111.37	2.8717	1.0320	0.1806	0.0307	0.0651
room5	131.64	142.32	2.5525	1.0384	0.0809	0.0189	0.0425
room6	67.27	130.83	4.2959	1.1324	0.2128	0.0150	0.0344

TABLE IV: RMSE OF ESTIMATED ANGULAR ACCELERATIONS AND TIME-VARYING BIASES OVER 20 TRIALS

trajectory	RMSE of Initial Guesses			RMSE of Final Estimates		
	$I_0 \boldsymbol{\alpha}$ [rad/s ²]	\mathbf{b}_a [m/s ² /√Hz]	\mathbf{b}_g [m/s ² · √Hz]	$I_0 \boldsymbol{\alpha}$ [rad/s ²]	\mathbf{b}_a [m/s ² /√Hz]	\mathbf{b}_g [m/s ² · √Hz]
room1	0.3147	9.6880×10^{-3}	7.5516×10^{-3}	0.1353	7.2235×10^{-3}	5.7869×10^{-4}
room2	0.2844	1.0285×10^{-2}	9.2693×10^{-3}	0.1256	5.9214×10^{-3}	1.0158×10^{-3}
room3	0.2940	1.0937×10^{-2}	7.8867×10^{-3}	0.1384	9.4185×10^{-3}	5.2697×10^{-4}
room4	0.2360	1.0516×10^{-2}	9.3446×10^{-3}	0.1297	5.3291×10^{-3}	5.6598×10^{-4}
room5	0.2331	1.1235×10^{-2}	9.6848×10^{-3}	0.1288	1.0378×10^{-2}	4.9971×10^{-4}
room6	0.2127	9.2290×10^{-3}	1.1778×10^{-2}	0.1370	7.7067×10^{-3}	5.2553×10^{-4}

TABLE V: RMSE OF IMU POSITION ESTIMATE AS A FUNCTION OF DIFFERENCE ($\delta \mathbf{p}$, $\delta \mathbf{q}$) BETWEEN INITIAL GUESS AND REFERENCE VALUE (UNIT: [MM])

$\delta \mathbf{q}$ [deg]	$\delta \mathbf{p}$ [mm]			
	0	10	20	30
0	0.1767	0.1763	0.1782	0.1765
30	0.1788	0.1787	0.1777	0.1783
60	0.1779	0.1773	0.1782	0.1772
90	39.3668	45.8379	29.9102	60.3195

TABLE VI: RMSE OF IMU ORIENTATION ESTIMATE AS A FUNCTION OF DIFFERENCE ($\delta \mathbf{p}$, $\delta \mathbf{q}$) BETWEEN INITIAL GUESS AND REFERENCE VALUE (UNIT: [DEG])

$\delta \mathbf{q}$ [deg]	$\delta \mathbf{p}$ [mm]			
	0	10	20	30
0	0.0223	0.0221	0.0223	0.0219
30	0.0226	0.0223	0.0222	0.0222
60	0.0223	0.0223	0.0223	0.0223
90	25.2160	5.7559	8.3864	18.6798

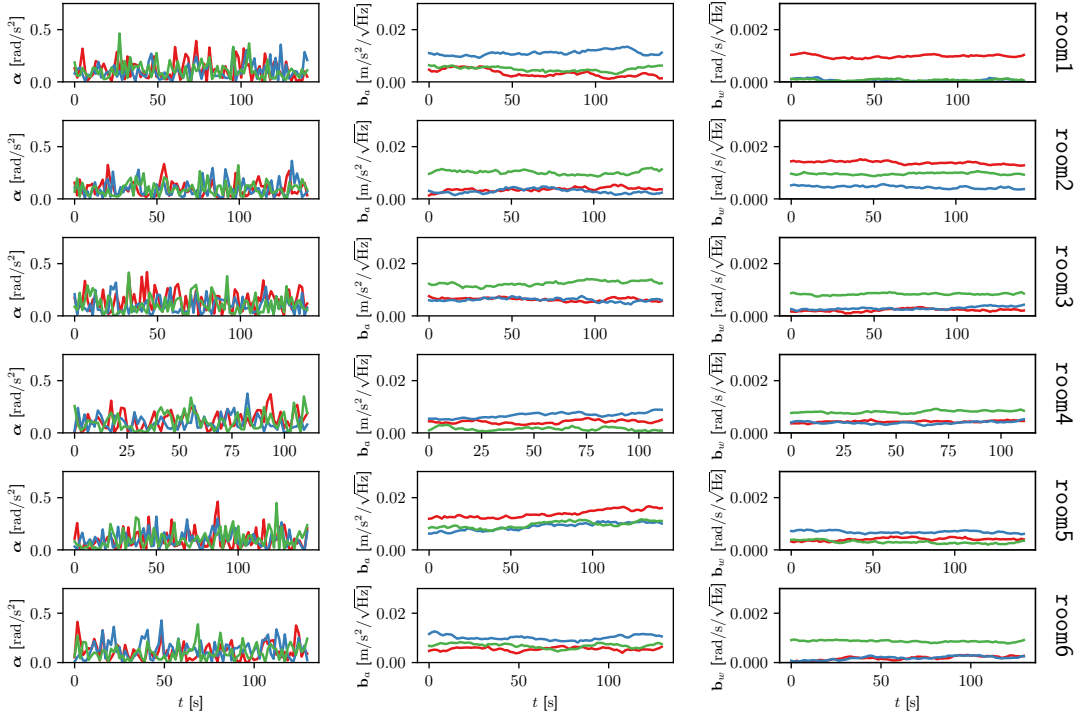


Fig. 2: Error of estimated angular acceleration and of each time-varying bias for the base IMU as functions of time over a single trial along six trajectories in simulation (red, green, blue are along x, y, and z axes, respectively).

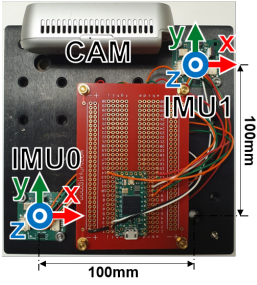


Fig. 3: Sensor rig used for hardware experiments.

CRM100 and CRM200). The camera was an Intel RealSense D435i. We emphasize that this camera was necessary to run Kalibr but was not needed by (and was not used by) our proposed method.

The noise and random walk characteristics of the accelerometers and the gyroscopes were found by analysis of Allan variance in the usual way [30], and were provided as input both to our method and to Kalibr. For the accelerometers, we obtained $\sigma_a = 1.13 \times 10^{-1} \text{ m/s}^2/\sqrt{\text{Hz}}$ and $\sigma_{b_a} = 2.54 \times 10^{-3} \text{ m/s}^2 \cdot \sqrt{\text{Hz}}$. For the gyroscopes, we obtained $\sigma_g = 3.74 \times 10^{-3} \text{ rad/s}/\sqrt{\text{Hz}}$ and $\sigma_{b_g} = 7.39 \times 10^{-5} \text{ rad/s} \cdot \sqrt{\text{Hz}}$. IMU measurements were all generated at 100 Hz but were not synchronized.

The intrinsic parameters of the camera (distortion, focal length, and principal point) were found using the camera calibration package from Intel that accompanies the D435i camera, and were provided as input to Kalibr (but not to our

method, which does not use camera images).

The intrinsic parameters of each IMU (scale factors and axis nonorthogonality) and the constant time offset were found by application of Kalibr itself to a preliminary dataset—distinct from the one we subsequently used to test extrinsic calibration—in which the sensor rig moved directly in front of a fiducial marker with excitation along all DOFs, as recommended by the authors of that method [13]. There are many other ways in which these intrinsic parameters and the time offset could have been obtained (and are obtained, in practice)—our choice to use Kalibr itself for intrinsic calibration and time synchronization was meant to make our subsequent evaluation of extrinsic calibration as favorable to Kalibr as possible, so as to provide a fair comparison with our proposed method. These intrinsic parameters and the time offset were provided as input both to our method and to Kalibr.

The reference positions and orientations used to compute errors in estimation of extrinsic calibration parameters were derived from the optical breadboard on which the IMUs were mounted. In particular, IMU0 and IMU1 were mounted 100 mm apart along the x and y axes, at the same position along the z axis, and at the same orientation—so, we assumed the following reference values:

$$\mathbf{p}_{I_1} = [0.1 \quad 0.1 \quad 0.0]^T \quad \mathbf{q}_{I_1} = [0 \quad 0 \quad 0 \quad 1]^T$$

We also assumed a reference value of zero gyroscope misalignment. We believe these are reasonable assumptions, given that the breadboard has an absolute hole-to-hole tolerance of ± 0.01 mm and a flatness tolerance of ± 0.15 mm

over 0.09 m^2 , and given that PCB manufacturing tolerances are typically sub-millimeter in position and sub-degree in orientation. However, we acknowledge that the reference positions and orientations we assumed are themselves a source of error in our experiments. As a consequence, we focus on establishing that both our method and Kalibr produce estimates that have “comparable” error with respect to these reference positions and orientations, rather than on rigorously establishing that our method produces “lower” error (at least in the baseline condition).

To collect data, we moved and rotated the sensor rig along a number of arbitrary trajectories, each lasting 60 seconds. To ensure a fair comparison between our method and Kalibr, we kept the calibration pattern in view of the camera during all of these trajectories. We collected data under three different conditions. In the *baseline* condition (21 trajectories), we used lighting that is known to work well with Kalibr. In the *blurry* condition (23 trajectories), we moved and rotated the rig much more quickly in a way that sometimes resulted in blurry images. In the *ill-lit* condition (21 trajectories), we used poor lighting that makes the calibration pattern less discernible by the Intel D435i camera.

B. Comparison of our method with Kalibr

Table VII shows the RMSE of the estimated extrinsic parameters—the relative position \mathbf{p}_{I_1} and orientation \mathbf{q}_{I_1} of IMU1 with respect to the base IMU0—over all trajectories in each condition, obtained both using Kalibr and using our proposed method. This table also shows the RMSE of gyroscope misalignment (relative to its assumed reference value) when each method is asked to include misalignment—and, in the case of Kalibr, also scale factors and axis non-orthogonality—in the set of parameters to be estimated. For both methods, the initial guess of relative position was the zero vector and the initial guess of relative orientation was the zero rotation. For both methods, when gyroscope misalignment was estimated, the initial guess of misalignment was the zero rotation. For our method, the initial guess of angular acceleration was found by numerical differentiation of gyroscope measurements from IMU0, and the initial guess of each time-varying bias was zero (same as for experiments in simulation). For both our method and Kalibr under the baseline condition, RMSE in position is on the order of millimeters and RMSE in orientation is on the order of degrees. The results shown provide evidence that our method matches the performance of Kalibr under the baseline condition regardless of whether or not each method is asked to estimate any other intrinsic parameters. We do note that, in contrast to simulation, the estimation of gyroscope misalignment (or other intrinsic parameters) seemed to make performance worse both for our method and for Kalibr, although this may be a result of incorrect reference values as discussed in the previous section.

Table VII also shows the success rate of each method under each condition. We define “success” as producing a result, regardless of its quality. For Kalibr, this means completion without any thrown errors. For our method,

this means convergence by Ceres Solver [31] without early termination. We define “success rate” as the ratio of successes to the total number of trajectories. The results shown provide evidence that Kalibr often fails in blurry or ill-lit conditions—note, as well, the corresponding increase in RMSE of estimated extrinsic calibration parameters even in those cases when Kalibr succeeds. Our method is, of course, unaffected by blurry or ill-lit conditions—but the fact that it succeeded across all three sets of trajectories with similar RMSE in all cases does provide evidence that our method is insensitive to the choice of trajectory.

Finally, Table VII shows the computation time required for each method using an octa-core Intel i7-10700 CPU operating at 2.90GHz with 32GB of RAM. We provide these results to benchmark future work and not to make any claims about the relative efficiency of our method, although we do note that it requires at most about 5 seconds to complete.

V. CONCLUSION

In this paper, we proposed an extrinsic calibration for a multi-IMU system using only measurements collected along arbitrary trajectories. We demonstrated the extent to which our method is insensitive to the choice of trajectories through simulations. We also substantiated that the proposed work shows comparable or even exceeds performance compared to a benchmark, which necessitates the use of a camera with a fiducial marker and accompanies its own failure cases.

In this paper, all accelerometer and gyroscope measurements collected along a calibration trajectory are used to compute the optimization cost function. However, it may not be necessary to use all of these measurements in the optimization process. In fact, there exists prior work that does select a subset of measurements for calibration [32], [33]. Future work along these lines may both improve the computation time of our method and may allow this method to be robust to particular degenerate motions (as we discussed in Section II-E).

In this work, we assumed sensors were time synchronized and had the same sample rates. Although there exist methods to synchronize sensors or to subsample the sensors collecting data at different rates, it would be more efficient to incorporate this into our extrinsic calibration process. It may even lead to more accurate extrinsic parameter estimates.

ACKNOWLEDGEMENT

This work was supported by the NASA Grant No. STTR-80NSSC20C0020.

REFERENCES

- [1] J.-O. Nilsson and I. Skog, “Inertial sensor arrays—a literature review,” in *IEEE European Navigation Conference (ENC)*, 2016.
- [2] I. Skog, J.-O. Nilsson, P. Händel, and A. Nehorai, “Inertial sensor arrays, maximum likelihood, and cramér-rao bound,” *IEEE Trans. Signal Process.*, vol. 64, no. 16, pp. 4218–4227, 2016.
- [3] K. Parsa, J. Angeles, and A. K. Misra, “Estimation of the flexural states of a macro-micro manipulator using point-acceleration data,” *IEEE Trans. Robot.*, vol. 21, no. 4, pp. 565–573, 2005.
- [4] I. B. Wijayasinghe, M. N. Saadatzi, S. Abubakar, and D. O. Popa, “A study on optimal placement of accelerometers for pose estimation of a robot arm,” in *IEEE International Conference on Robotics and Automation (ICRA)*, 2018, pp. 1444–1451.

TABLE VII: RMSE OF ESTIMATED EXTRINSIC PARAMETERS, COMPUTATION TIME, AND SUCCESS RATE FOR BOTH KALIBR AND OUR METHOD WHEN APPLIED TO DATA FROM HARDWARE EXPERIMENTS

condition	Kalibr		Our Method	
	Without Estimation of Intrinsic Parameters	With Estimation of Intrinsic Parameters	Without Estimation of Gyroscope Misalignment	With Estimation of Gyroscope Misalignment
<i>baseline</i>	RMSE in \mathbf{p} [mm]	3.64	4.39	1.63
	RMSE in \mathbf{q} [deg]	0.61	1.35	0.63
	RMSE in ${}^g_I\mathbf{q}$ [deg]	-	2.06	-
	computation time [ms]	56.15 ± 6.49	106.96 ± 16.34	3.62 ± 0.40
<i>blurry</i>	success rate	19 / 21	19 / 21	21 / 21
	RMSE in \mathbf{p} [mm]	3.48	70.41	1.88
	RMSE in \mathbf{q} [deg]	0.69	26.98	0.68
	RMSE in ${}^g_I\mathbf{q}$ [deg]	-	30.67	-
<i>ill-lit</i>	computation time [ms]	58.67 ± 11.36	98.99 ± 12.27	4.04 ± 0.47
	success rate	13 / 23	14 / 23	23 / 23
	RMSE in \mathbf{p} [mm]	119.96	107.42	1.51
	RMSE in \mathbf{q} [deg]	3.30	1.81	0.68
<i>ill-lit</i>	RMSE in ${}^g_I\mathbf{q}$ [deg]	-	1.03	-
	computation time [ms]	8.67	7.83 ± 0.28	3.91 ± 0.44
	success rate	1 / 21	2 / 21	21 / 21
				5.16 ± 0.55

- [5] M. Zhang, X. Xu, Y. Chen, and M. Li, “A lightweight and accurate localization algorithm using multiple inertial measurement units,” *IEEE Robot. Autom. Lett.*, vol. 5, no. 2, pp. 1508–1515, 2020.
- [6] K. Eckenhoff, P. Geneva, and G. Huang, “Sensor-failure-resilient multi-imu visual-inertial navigation,” in *IEEE International Conference on Robotics and Automation (ICRA)*, 2019, pp. 3542–3548.
- [7] ———, “Mimc-vins: A versatile and resilient multi-imu multi-camera visual-inertial navigation system,” *IEEE Trans. Robot.*, vol. 37, no. 5, pp. 1360–1380, 2021.
- [8] S. Y. Cho and C. G. Park, “A calibration technique for a redundant imu containing low-grade inertial sensors,” *ETRI journal*, vol. 27, no. 4, pp. 418–426, 2005.
- [9] P. Schopp, L. Klingbeil, C. Peters, and Y. Manoli, “Design, geometry evaluation, and calibration of a gyroscope-free inertial measurement unit,” *Sensors and Actuators A: Physical*, vol. 162, no. 2, pp. 379–387, 2010.
- [10] K. He, J. Han, and Y. Shao, “A novel redundant inertial measurement unit and calibration algorithm,” in *IEEE International Conference on Optoelectronics and Microelectronics (ICOM)*, 2013, pp. 18–23.
- [11] J.-O. Nilsson, I. Skog, and P. Händel, “Aligning the forces—eliminating the misalignments in imu arrays,” *IEEE Trans. Instrum. Meas.*, vol. 63, no. 10, pp. 2498–2500, 2014.
- [12] P. Furgale, J. Rehder, and R. Siegwart, “Unified temporal and spatial calibration for multi-sensor systems,” in *IEEE/RSJ International Conference on Intelligent Robots and Systems*, 2013, pp. 1280–1286.
- [13] J. Rehder, J. Nikolic, T. Schneider, T. Hinzmman, and R. Siegwart, “Extending kalibr: Calibrating the extrinsics of multiple imus and of individual axes,” in *IEEE International Conference on Robotics and Automation (ICRA)*, 2016, pp. 4304–4311.
- [14] K. Qiu, T. Qin, J. Pan, S. Liu, and S. Shen, “Real-time temporal and rotational calibration of heterogeneous sensors using motion correlation analysis,” *IEEE Trans. Robot.*, 2020.
- [15] D. Kim, S. Shin, and I. S. Kweon, “On-line initialization and extrinsic calibration of an inertial navigation system with a relative preintegration method on manifold,” *IEEE Trans. Autom. Sci. Eng.*, vol. 15, no. 3, pp. 1272–1285, 2017.
- [16] P. Schopp, H. Graf, W. Burgard, and Y. Manoli, “Self-calibration of accelerometer arrays,” *IEEE Trans. Instrum. Meas.*, vol. 65, no. 8, pp. 1913–1925, 2016.
- [17] H. G. Kortier, “In use imu calibration and pose estimation..,” in *IPIN (Short Papers/Work-in-Progress Papers)*, 2019, pp. 195–202.
- [18] P. Geneva, K. Eckenhoff, W. Lee, Y. Yang, and G. Huang, “Open-vins: A research platform for visual-inertial estimation,” in *IEEE International Conference on Robotics and Automation (ICRA)*, 2020, pp. 4666–4672.
- [19] D. Tedaldi, A. Pretto, and E. Menegatti, “A robust and easy to implement method for imu calibration without external equipments,” in *IEEE International Conference on Robotics and Automation (ICRA)*, 2014, pp. 3042–3049.
- [20] O. Särkkä, T. Nieminen, S. Suuriniemi, and L. Kettunen, “A multi-position calibration method for consumer-grade accelerometers, gyroscopes, and magnetometers to field conditions,” *IEEE Sensors J.*, vol. 17, no. 11, pp. 3470–3481, 2017.
- [21] L. Ye, Y. Guo, and S. W. Su, “An efficient autocalibration method for triaxial accelerometer,” *IEEE Trans. Instrum. Meas.*, vol. 66, no. 9, pp. 2380–2390, 2017.
- [22] X. Li and Z. Li, “Vector-aided in-field calibration method for low-end mems gyros in attitude and heading reference systems,” *IEEE Trans. Instrum. Meas.*, vol. 63, no. 11, pp. 2675–2681, 2014.
- [23] M. Hwangbo, J.-S. Kim, and T. Kanade, “Inertial-aided klt feature tracking for a moving camera,” in *IEEE/RSJ International Conference on Intelligent Robots and Systems*, 2009, pp. 1909–1916.
- [24] I. Skog, J.-O. Nilsson, and P. Händel, “An open-source multi inertial measurement unit (mimu) platform,” in *International Symposium on Inertial Sensors and Systems (ISISS)*, 2014.
- [25] G. Coville and G. Avitabile, “Multiple synchronized inertial measurement unit sensor boards platform for activity monitoring,” *IEEE Sensors J.*, vol. 20, no. 15, pp. 8771–8777, 2020.
- [26] C. Jauffret, “Observability and fisher information matrix in nonlinear regression,” *IEEE Trans. Aerosp. Electron. Syst.*, vol. 43, no. 2, pp. 756–759, 2007.
- [27] J. Kelly and G. S. Sukhatme, “Visual-inertial sensor fusion: Localization, mapping and sensor-to-sensor self-calibration,” *The International Journal of Robotics Research*, vol. 30, no. 1, pp. 56–79, 2011.
- [28] F. M. Mirzaei and S. I. Roumeliotis, “A kalman filter-based algorithm for imu-camera calibration: Observability analysis and performance evaluation,” *IEEE Trans. Robot.*, vol. 24, no. 5, pp. 1143–1156, 2008.
- [29] D. Schubert, T. Goll, N. Demmel, V. Usenko, J. Stueckler, and D. Cremers, “The tum vi benchmark for evaluating visual-inertial odometry,” in *IEEE/RSJ International Conference on Intelligent Robots and Systems (IROS)*, Oct. 2018.
- [30] N. El-Sheemy, H. Hou, and X. Niu, “Analysis and modeling of inertial sensors using allan variance,” *IEEE Trans. Instrum. Meas.*, vol. 57, no. 1, pp. 140–149, 2008.
- [31] S. Agarwal, K. Mierle, et al., “Ceres solver,” 2012.
- [32] T. Schneider, M. Li, C. Cadena, J. Nieto, and R. Siegwart, “Observability-aware self-calibration of visual and inertial sensors for ego-motion estimation,” *IEEE Sensors J.*, vol. 19, no. 10, pp. 3846–3860, 2019.
- [33] J. Maye, P. Furgale, and R. Siegwart, “Self-supervised calibration for robotic systems,” in *IEEE Intelligent Vehicles Symposium (IV)*, 2013, pp. 473–480.